Journal of Colloid and Interface Science 362 (2011) 118–126

Contents lists available at ScienceDirect

Journal of Colloid and Interface Science

www.elsevier.com/locate/jcis

Fibrinogen stability under surfactant interaction

Natalia Hassan [a], Leandro R.S. Barbosa [b], Rosangela Itri [b,*], Juan M. Ruso [a,*]

[a] Soft Matter and Molecular Biophysics Group, Department of Applied Physics, University of Santiago de Compostela, Campus Vida s/n, 15782 Santiago de Compostela, Spain
[b] Instituto de Física, Universidade de Sao Paulo, Cx. Postal 66318, CEP 05315-970, Sao Paulo, SP, Brazil

ARTICLE INFO

Article history:
Received 9 March 2011
Accepted 2 June 2011
Available online 15 June 2011

Keywords:
Fibrinogen
Fluorinated
Hydrogenated
DSC
SAXS

ABSTRACT

Differential scanning calorimetry (DSC), circular dichroism (CD), difference spectroscopy (UV–vis), Raman spectroscopy, and small-angle X-ray scattering (SAXS) measurements have been performed in the present work to provide a quantitatively comprehensive physicochemical description of the complexation between bovine fibrinogen and the sodium perfluorooctanoate, sodium octanoate, and sodium dodecanoate in glycine buffer (pH 8.5). It has been found that sodium octanoate and dodecanoate act as fibrinogen destabilizer. Meanwhile, sodium perfluorooctanoate acts as a structure stabilizer at low molar concentration and as a destabilizer at high molar concentration. Fibrinogen's secondary structure is affected by all three studied surfactants (decrease in α-helix and an increase in β-sheet content) to a different extent. DSC and UV–vis revealed the existence of intermediate states in the thermal unfolding process of fibrinogen. In addition, SAXS data analysis showed that pure fibrinogen adopts a paired-dimer structure in solution. Such a structure is unaltered by sodium octanoate and perfluoroctanoate. However, interaction of sodium dodecanoate with the fibrinogen affects the protein conformation leading to a complex formation. Taken together, all results evidence that both surfactant hydrophobicity and tail length mediate the fibrinogen stability upon interaction.

1. Introduction

In the last decade, a significant amount of different proteins have been applied to several nanotechnology applications as biomimetic materials, tissue engineering, printing of proteins, drug delivery, bioelectronics and nanoparticle patterning [1–3]. Certainly, the interactions between small molecules with proteins affect their respective biological functions and determine their stability in solution with respect to aggregation, liquefaction, and other phase transformations. Furthermore, the pathways of protein aggregation, crystal formation, folding, or unfolding are largely defined by the forces acting between the molecules [4]. The understanding of molecular recognition in protein–ligand complexes is crucial to better comprehend the associated biological function and of practical importance in the discovery, for instance, of new drugs. The weak, noncovalent interactions (hydrophobic, electrostatic, van der Waals, and hydrogen bonding) govern the ligand-binding process. Elucidating the role of these interactions concomitantly with the involved time scales must provide insights into the mechanism of molecular recognition and the role of binding cooperativity in the protein dynamics [5].

Fibrinogen is a complex multidomain protein whose major function is to form fibrin clots that prevent the loss of blood upon vascular injury. Bovine fibrinogen (340 kDa) is a 45-nm-long (with an approximate diameter of 5 nm) disulfide-linked dimer of three nonidentical polypeptide chains, Aα, Bβ, and γ. The NH_2 terminal portions of the six chains are linked together in the central region of the molecule by 11 disulfide bonds forming a small globular domain, the so-called disulfide knot, in the center [6,7]. The C-termini of each of the three chains end in globular domains, and those of the Bβ and γ chains are located at the ends of the molecule. Cleavages in all three chains then yield two D domains and one E domain. The E domain consists of the NH_2 terminal regions of α-, β-, and γ-chains chains held together by disulfide bonds. The majority of the D region is formed by the C-terminal portions of the β- and γ-chains folded into similar structures. The COOH-terminal portion of each fibrinogen Aα chain forms a compact αC-domain attached to the bulk of the molecule with a flexible αC-connector (see Fibrinogen Scheme 1).

In addition, fibrinogen shows a unique characteristic in its folding. According to the current view, in fibrinogen, two αC-domains interact intramolecularly with each other and with the central region of the molecule, while in fibrin, they switch to an intermolecular interaction to form αC-polymers. This structural organization involves fibrinogen in fibrin assembly process and promotes cell adhesion and migration through their RGD sequences [8].

Contemporary studies have been centered on the use of fibrinogen for nonviral vector delivery [9], scaffolds [10], and

* Corresponding authors.
E-mail addresses: itri@if.usp.br (R. Itri), juanm.ruso@usc.es (J.M. Ruso).

0021-9797/$ - see front matter © 2011 Elsevier Inc. All rights reserved.
doi:10.1016/j.jcis.2011.06.010

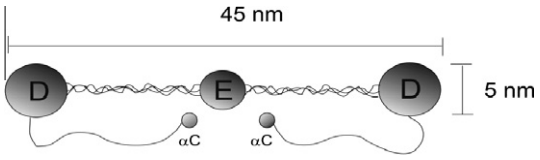

Scheme 1. Fibrinogen scheme.

biocompatibility studies [11,12]. Despite the very interesting applications of this protein, its interaction with small molecules as surfactants has not been exploited yet. It is well known that surfactants can denature proteins at smaller molar ratio than that required by weakly binding chemical denaturants such as guanidinium chloride or urea. Even the binding of a restrict number of surfactant molecules can induce substantial conformational changes, since the surfactants can wedge themselves into the interior of the protein. Structural studies of proteins interacting with surfactants at sub-denaturation concentrations reveal that the high affinity is achieved by a combination of electrostatic and hydrophobic interactions. As a rule, most proteins follow the same sequence of binding events: initial interaction between surfactants [13] and proteins, partial unfold, exposing of more binding sites, and subsequent expansion of the polypeptide chain. However, the exact number of binding events and associated conformational changes will depend on the structure and amino acid composition of the protein in question [14–16].

We have focused our research on the interactions between proteins and surfactants with a view of better understanding the mechanisms that are responsible for the adsorption of amphiphile molecules to biopolymers [15,17]. In particular, fluorinated surfactants are considered less denaturing for proteins than their hydrocarbon-base counterparts [18]. Understanding the possible interactions that occur between fluorinated surfactants and proteins can be helpful to guide the design of new systems for gel electrophoresis applications [16]. Recently, the interaction between such surfactants and proteins has also received great attention because it has been shown that fluorinated surfactants can control the insertion of pore-forming proteins in lipid membranes [19]. In this way, it is very important to explore and to understand the physicochemical properties of hydrocarbon/fluorocarbon surfactant in the presence of proteins.

In this sense, the current work is undertaken to investigate the stability, interactions, and possible conformational changes in bovine fibrinogen in the presence of different surfactants. Sodium perfluorooctanoate, sodium octanoate, and sodium dodecanoate have been chosen because their solution properties have been widely characterized in previous works. Furthermore, these surfactants allow us to compare the differences between hydrocarbon and fluorocarbon surfactants with the same alkyl chain with those where the hydrocarbon chain is 1.5 times longer than the fluorocarbon chain. (It is well known that in this relation both surfactants have similar critical micellar concentration, 27 mM and 30 mM for sodium dodecanoate and sodium perfluorooctanoate, respectively, whereas cmc = 380 mM for sodium octanoate [20]). To this end, we made use of differential scanning calorimetry to get insight into thermodynamic parameters, absorbance spectroscopy, and circular dichroism to infer about changes in the protein secondary structure as well as small-angle X-ray scattering to have information on protein conformational changes. Interestingly, we observed that sodium octanoate and perfluorooctanoate do not affect the fibrinogen conformation. Such findings could be of interest for applications in biomaterial science where devices should be created with improved hemocompatibility.

2. Materials and methods

2.1. Materials

Bovine plasma fibrinogen, fraction I, type IV, was purchased from Sigma and used without purification. Sodium octanoate (C_8HONa) and sodium perfluorooctanoate (C_8FONa) were obtained from Lancaster Synthesis Ltd. Sodium dodecanoate ($C_{12}HONa$) with purity over 99% was obtained from Sigma Chemical Co. The buffer solution consisted of 50 mN glycine and adjusted sodium hydroxide to give a pH value of 8.5. Samples were prepared within 2 h prior to usage. All chemical reagents were of analytical grade, and solutions were made using doubly distilled and degassed water.

2.2. Differential scanning calorimetry

Differential scanning calorimetry (DSC) measurements were taken using a VP-DSC (MicroCal Inc., Northampton, MA) calorimeter with 0.542 ml twin cells for the reference and sample solutions. Prior to the DSC experiments, the samples and the references were degassed under vacuum while being stirred. Thermograms were recorded between 20 and 110 °C at a scan rate of 60 °C per hour. Each experiment was conducted in triplicate to check the reproducibility. The baseline reference, obtained with both cells filled with buffer, was subtracted from the thermograms of the samples. The heat capacity curves were evaluated using the MicroCal Origin 7.0 software provided with the equipment to obtain ΔH and T_m values.

2.3. Difference spectroscopy

Difference spectra were measured using a Beckman spectrophotometer (model DU 640), with six microcuvettes, which operates in the UV–vis region. All measurements were taken using fibrinogen solutions with a fixed concentration of 0.5 g dm^{-3} in carefully matched quartz cuvettes (50 µl capacity). For absorbance difference spectra, just two cells were used. The first microcuvette containing just protein in the buffer solution was used as a blank reference; meanwhile, the other one was filled with fibrinogen in the presence of surfactant solution. The microcuvettes were then placed in the same orientation for all the tests. Measurements were taken under the condition that protein and surfactant had been incubated for over 2 h, after which the difference spectra did not change. For absorbance measurements with varying temperature, a Beckman (DU Series) temperature controller was used, following the Peltier methods of controlling temperature, in the range of 25–80 °C.

2.4. Circular dichroism

Far-UV circular dichroism (CD) spectra were obtained using a JASCO-715 automatic recording spectropolarimeter (Japan) with a JASCO PTC-343 Peltier-type thermostated cell holder. Quartz cuvettes with 0.2-cm pathlength were used. CD spectra of pure fibrinogen and fibrinogen-surfactants dilute solutions were recorded from 190 to 270 nm. Protein concentration was 0.5 g dm^{-3}, and surfactant concentrations varied from 1 to 10 mM. The following setting was used: resolution, 1 nm; bandwidth, 1 nm; sensitivity, 50 mdeg; response time, 8 s; accumulation, 3; and scan rate 50 nm/min. Corresponding absorbance contributions from buffer solution was subtracted with the same instrumental parameters. Data are reported as molar ellipticity and determined as

$$[\theta]_\lambda = \frac{\theta_\lambda M_r}{Ncl} \quad (1)$$

where c is the protein concentration, l is the pathlength of the cell, $[\theta]_\lambda$ is the measured ellipticity at a wavelength λ, M_r is the molecular mass of the protein, and N is the number of residues. The secondary structure content was analyzed by Dichroweb program [21] using CONTIN algorithm.

2.5. Raman spectroscopy

The Raman scattering measurements were taken using a Raman microprobe instrument consisting of a Jobin–Yvon T64000 spectrometer equipped with a microscope, which allows a spatial resolution on the sample of about 1 μm. The Raman signal was detected by a multichannel CCD detector cooled with liquid nitrogen. Raman spectra over the whole optical frequency range were recorded using the subtractive configuration of the spectrometer, with a spectral resolution of about 2 cm^{-1}. To improve the resolution of closely spaced peaks, high-resolution scans of some frequency regions were recorded using the triple additive configuration, with a spectral resolution better than 1 cm^{-1}. The light was collected in backscattering geometry through an objective of numerical aperture 0.95. The 785 nm line of an Ar^+ laser was used as excitation, focused on a spot of ≈1 μm in diameter, with an incident power on the sample of ≈2 mW.

2.6. Small-angle X-ray scattering (SAXS)

The experiments were performed in a commercially available NanoStar small-angle X-ray instrument (Bruker AXS) with Cu Kα_1 radiation (λ = 1.54 Å), sample-to-detector distance of ∼650 mm. The scattering data were collected by a two-dimensional position sensitive gas detector (HiSTAR) over a scattering vector of q (=$(4\pi\sin\theta)/\lambda$, being 2θ the scattering angle) ranging from q_{min} = 0.013 $Å^{-1}$ to q_{max} = 0.33 $Å^{-1}$. The q_{min} value allowed us to determine the macromolecules' maximum dimension, D_{max}, of ca. 480 Å ($D_{max} = 2\pi/q_{min}$) that is compatible to FB longest axis, and q_{max} allowed us to monitor the micelles' formation concomitantly. Samples were conditioned in glass capillaries with 2.0 mm inner-diameter, perpendicular to the incident X-ray beam. Data collection took from 2 to 4 h, according to protein concentration. No radiation damage was observed. The obtained scattering curves were corrected for buffer scattering and sample attenuation.

It is well known that the scattering intensity from a set of monodisperse particles randomly distributed is given by [22]

$$I(q) = \gamma n_p P(q) S_M(q) \quad (2)$$

where γ is a calibration factor related to the experimental setup and n_p corresponds to the particle number density. $P(q)$ is the scattering particle form factor that depends on the electron density contrast between the particle and the surrounding medium, and $S_M(q)$ is the so-called 'measured' structure factor, which is equal to 1 for noninteracting particles. In the current work, we made use of the human fibrinogen crystallographic structure (code: 3GHG from PDB website) to calculate the protein form factor $P(q)$ by Monte Carlo simulations (MCS), as previously described [22].

Concerning micellar aggregates in solution, $P(q)$ was calculated supposing that the micelle resembles small prolate ellipsoids [23]. In this way, the ellipsoid shortest semi-axis is on the order of paraffinic chain length, R_{par}, whereas the largest semi-axis is vR_{par}, with v equal to the micellar axial ratio. The model assumes that the micelle is constituted by two shells of different electron densities: an inner core of paraffinic moiety, with electron density ρ_{par}, and an external shell, surrounding the core, with a respective polar headgroup thickness σ that includes the hydration water and with electron density ρ_{pol}, relative to the continuous medium (buffer solution with electron density similar to that of water ρ_w = 0.334 e/$Å^3$). $S_M(q)$ function was modeled according to the well-known *Mean Spherical Approximation* (MSA) [24]. In this methodology, the micelles are treated as charged spheres interacting through a screened-Coulomb potential (the repulsive contribution of the DLVO potential). The fitting parameters of such procedure are: the amount of charges on the micelle surface (ionization coefficient, α) and the effective diameter of the sphere. Details of this methodology can be found elsewhere [23].

For micelles interacting with fibrinogen, we analyzed the SAXS curve through the pair distribution function, $p(r)$, according to the procedure recently reported for protein complexes with sodium alkyl sulfates [16]. Such a function is a Fourier transform of the scattering intensity $I(q)$, which gives information about the scattering particle shape and maximum dimension [25]. In the case of micelles associated with polypeptide chains, it has been shown that three structural parameters can be retrieved directly from $p(r)$. These are the average length of the complex, the micelle radius, and the distance between neighboring micelles [16]. In this work, the $p(r)$ function was calculated by means of a generalized indirect Fourier transform (GIFT software) developed by Glatter et al. [26].

3. Results and discussion

3.1. DSC, CD, absorbance difference, and Raman spectroscopy: samples containing 0.5 g dm^{-3} of fibrinogen in the absence and presence of surfactant concentration below cmc

A first set of DSC experiments at different protein concentrations (from 0.1 to 4 g dm^{-3}) have been performed and revealed that the concentration does not influence on the main features of the thermograms. On the other hand, three thermograms were obtained from some samples at different scan-rates (45, 60 and 90 °C per hour) and showed that the temperature corresponding to the maximum heat capacity is scan-rate-dependent (from 52.58 to 53.32 °C for the lowest to the highest scan rate, respectively). This fact indicates that the fibrinogen denaturation process is kinetically controlled [27]. Therefore, we decided to perform the scans at 60 °C per hour.

A DSC scan of fibrinogen (0.5 g dm^{-3}) in buffer solution (glycine, pH 8.5) is shown in Fig. 1A. Three endothermic peaks can be observed. The narrow and symmetrical peaks located at 52.85 and 93.97 °C have been attributed to the denaturation of the end D and central E fragments of fibrinogen, respectively [28,29]. On the other hand, the small and broad peak at 76.62 °C has been related to the denaturation of the C-terminal of the Aα chains [27].

The reversibility of the transitions was checked by heating the samples in the calorimetric cell after cooling them down from the first run. Consecutive scans show no peaks because of total fibrinogen denaturation after heating. However, with the aim of investigating the reversibility of each endothermic peak, we performed distinct heating and cooling cycles as follows. Firstly, the sample was heated up to 60 °C, cooled down to room temperature, and reheated up to 110 °C (Fig. 1B-II). As one can see, the first peak disappeared showing the irreversibility of such a transition. Similarly, the other two calorimetric peaks also disappeared after heating and cooling processes as displayed in the Fig. 1B-III and IV. Consequently, all calorimetric peaks were found to be irreversible under temperature. Thus, only the first scan is shown for each studied sample.

The DSC thermograms from fibrinogen in the surfactant-containing solutions are shown in Fig. 2. In all studied systems, no reversibility was found as in the case of pure fibrinogen. The thermodynamic characteristics of the thermal denaturation, namely, melting temperatures (T_m, temperatures at which a maximum occurred in the endothermic peaks), calorimetric enthalpy

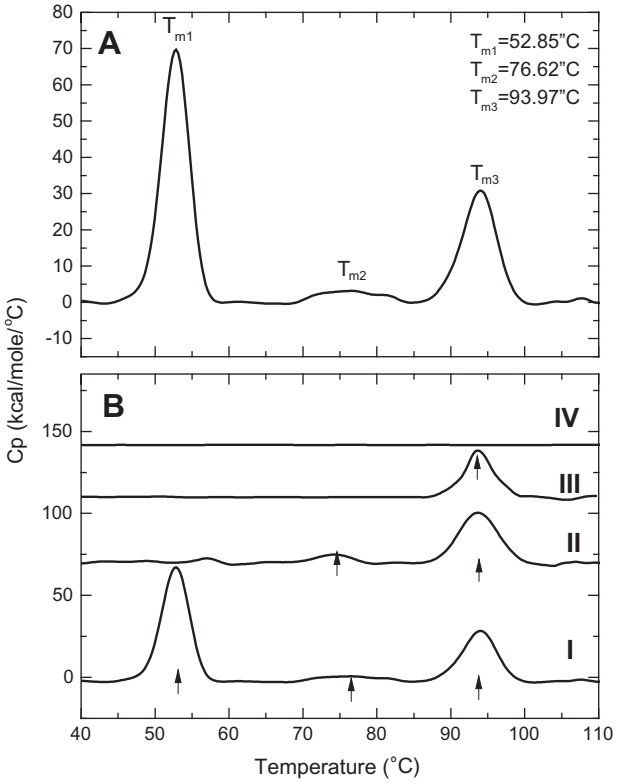

Fig. 1. (A) Heat capacity curve of fibrinogen (0.5 g dm^{-3}) in buffer solution, pH 8.5; (B) heat capacity curves of fibrinogen: (I) first scan; (II) heating up to 60 °C, cooled down, and heated up again; (III) heating up to 85 °C, cooled, and heated again; (IV) heating up to 98 °C, cooled, and heated again. The thermograms were vertically displaced for clarity.

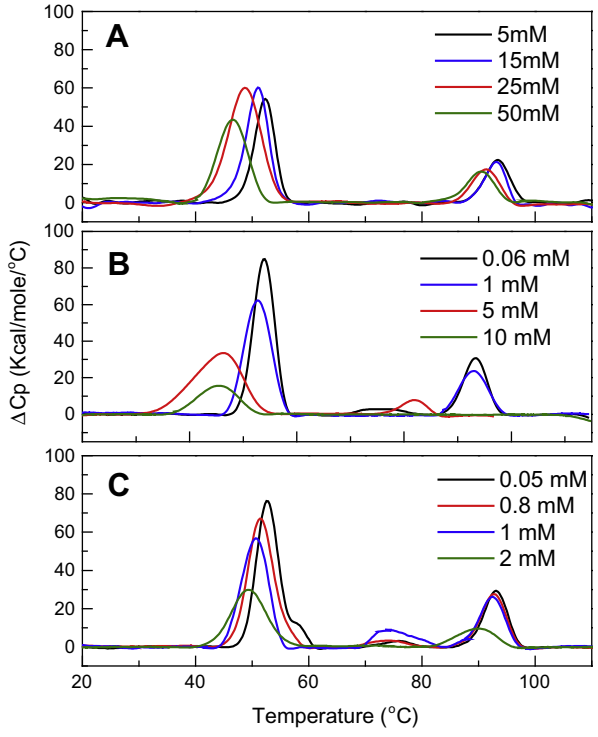

Fig. 2. DSC thermograms of fibrinogen (0.5 g dm^{-3}) in the presence of (A) C_8HONa, (B) C_8FONa, and (C) C_{12}HONa.

(ΔH), van't Hoff enthalpy (ΔH_v), and cooperativity (n, the ratio of calorimetric enthalpy to van't Hoff enthalpy) were obtained and listed in Table 1.

As one can note, with increasing hydrogenated surfactant concentration, endothermic peaks shift to lower temperatures or disappear as in the case of the second peak in respect to pure fibrinogen. Significant changes in the peaks features are induced by the highest surfactant concentrations. Regarding the effect of the fluorinated surfactant, the first endothermic peak shifts to higher temperatures up to 1 mM C_8FONa concentration (acting as a stabilizer), followed by a decrease in T_m afterwards. This behavior may be attributed to the effect of the CF_3 group on the hydration shell of the peptides. This fact has been interpreted on the basis that small amount of surfactants must induce a protective effect due to some binding function of the surfactant ions. In other words, the native conformation is stabilized by a cross-linking function of the surfactant between a group of nonpolar residues and a positively charged residue located on different loops of the protein [30]. The first peak thus becomes broader, and the second and third ones disappear when C_8FONa is present at high concentrations. Concomitantly, the heat capacity varies with surfactant concentration.

This first set of measurements points out a decrease in stability of fibrinogen with increase in the surfactant concentration. Such a fact has been previously observed in other systems; when surfactant concentration is increased, hydrophobic interactions become more dominant, and surfactant hydrophobic moieties will tend to penetrate into the hydrophobic domains of the protein in order to reduce their contacts with water. Thus, due to such a penetration, the protein may change its conformation somewhat, which results in a lower thermal stability [31].

Enthalpies of the protein thermal denaturation exhibit the highest values for the first peak, whereas values for the second are the lowest (Table 1). In the presence of C_8FONa and C_{12}HONa, these values tend to decrease with the surfactant concentration. However, with C_8HONa, such a behavior is only corroborated for the third peak. Comparing the values among the different systems, one can notice that the enthalpies increase in the order of C_8HONa < C_{12}HONa < C_8FONa.

Concerning cooperativity, n, it depends on a number of factors. When estimated values of van't Hoff enthalpy for a particular reaction are compared with enthalpy values obtained directly by calorimetric methods, substantial disagreement between both values often takes place. Such discrepancies have been suggested to indicate that unfolding is more complex than the simple one-to-one model used to describe the data. It has been noted that binding reactions can include the displacement of solvent and counterions, as well as other linked equilibria such as protonation or conformational changes. It has been suggested that calorimetric enthalpy includes these contributions, which are not observed in the van't Hoff method. This suggests that the van't Hoff enthalpy is the "intrinsic" binding heat, whereas the calorimetric enthalpy includes other concomitant reactions (i.e., linked equilibria). Thus, when $n > 1$, the unfolding is not a two-state process but involves unfolded intermediates or independent domains significantly populated. In the case of $n < 1$, this implies that the overall protein is not correctly folded (probably due to irreversible or aggregation effects). For all studied systems, one can conclude that $n > 1$ for the first peak and $n < 1$ for the second and third ones. This implies that one or more intermediate states are populated in the lowest temperature change, while denaturation at higher temperatures involves intermolecular cooperation [32].

In order to get more information about changes in the fibrinogen secondary structure, we have also performed measurements of circular dichroism and absorbance difference as described below.

Table 1
Thermodynamic parameters obtained from DSC thermograms of fibrinogen in the presence of C_8FONa, C_8HONa, and C_{12}HONa.

	T_m (°C)			ΔH (kcal/mol)			ΔH_v (kcal/mol)			Cooperativity		
	T_{m1}	T_{m2}	T_{m3}	ΔH_1	ΔH_2	ΔH_3	ΔH_{v1}	ΔH_{v2}	ΔH_{v3}	n_1	n_2	n_3
Surfactant-free	52.7	74.5	93.9	288.2	34.2	156.1	179.4	122.4	186.3	1.61	0.28	0.84
C_8FONa (mM)												
0.06	53.8	75.7	93.2	416.3	24.5	167.5	182.9	126.8	202.6	2.27	0.19	0.82
0.08	54.2	76.8	93.2	475.0	76.5	195.8	167.0	47.0	182.7	2.84	1.62	1.07
0.2	54.1	74.7	93.2	429.5	35.9	181.0	178.0	103.7	190.0	2.41	0.34	0.95
0.5	53.4		93.2	391.3		184.6	180.6		183.2	2.11		1.00
0.8	53.6		93.2	364.3		148.1	182.1		199.5	2.00		0.74
1	53.0		93.2	372.8		153.0	176.8		194.9	2.10		0.78
1.5	52.8		93.1	306.7		142.4	182.3		196.4	1.68		0.72
3	51.9		88.0	278.9		42.4	138.6		186.7	2.01		0.22
5	45.3		81.7	185.8		43.3	113.6		183.4	1.63		0.22
10	45.2			143.3			89.6			1.59		
C_8HONa (mM)												
1	52.2		93.4	190.3		137.5	191.8		170.0	0.99		0.80
5	52.1		93.2	250.8		123.7	185.8		195.8	1.34		0.63
15	50.8		92.8	309.6		99.4	163.4		235.0	1.89		0.42
25	49.6		92.2	444.9		99.7	118.4		209.0	3.75		0.47
50	47.5		91.3	289.9		100.7	132.9		186.7	2.18		0.53
C_{12}HONa (mM)												
0.05	53.0	75.8	93.2	390.1	17.9	152.1	166.0	166.5	209.1	2.35	0.10	0.72
0.2	51.7	74.3	93.7	298.6	44.1	157.1	154.4	93.5	201.5	1.93	0.47	0.77
0.8	51.7	74.2	92.8	392.2	24.9	151.1	151.6	136.7	209.3	2.58	0.18	0.72
1	50.5	74.9	92.3	336.2	75.6	145.6	144.0	118.6	196.0	2.33	0.63	0.75
2	49.4		89.5	234.6		78.1	108.7		136.7	2.15		0.57

Chen et al. [27] have estimated that the native fibrinogen molecule contains about 35% α-helix, 21% β-sheets, 13% β-turn, and 31% random coil. Other authors have estimated 42% α-helix, 7% β-sheets, 20% β-turn, and 30.8% random coil [33]. However, the trends are clear: with increasing temperature, α-helix and β-sheets change little before the onset of the first peak but change dramatically (α-helix decreased and β-sheets increased) in the range of 55–65 °C. After this, α-helix contents decrease moderately and finally an important decrease is observed from 80 to 100 °C. This behavior indicates that the decrease in α-helix occurs in domain E and in the coiled-coil portion of fragment D [28]. Some authors have found that the decrease in α-helix content is due to a conformational change to a β-structure, on the basis that the ellipticity of the negative peaks in the CD spectrum for fibrinogen changed from more to less negative values and their observation that the fluorescence intensity decreased [34].

Here, we make use of CD measurements on fibrinogen solutions containing surfactants at different temperatures (40, 70, and 90 °C) (see Fig. 3). The first temperature corresponds to the area below the first calorimetric peak (native fibrinogen structure), the second is placed between the second and third peaks (just D domain is unfolded), and the final one is located over the third peak. Fragment D contains a distribution of secondary structure values of 35% α-helix, 29% β-sheet segments, and 17% turn structures. Fragment D has two domains: a portion of the original coiled-coil and also a thermally labile globular domain. The coiled-coil portion showed an α-helical content around 70%, and the globular domain is estimated to be rich in β-sheet structures. Fragment E is shown to contain 50% α-helical values, attributed to its coiled-coil portions, and minor β-strands, and turn structures [35].

From our results, we can estimate that the native fibrinogen molecule at 40 °C contains about 30% α-helix and 18% β-sheets. Furthermore, all three surfactants interact with fibrinogen and affect the protein secondary structure to a different extent. At 40 °C, changes in secondary structure are insignificant for surfactant concentrations below 3 mM. However, by heating up the samples (70 and 90 °C), greater changes take place at lower surfactant concentrations. The backbone hydrogen bonds of α-helix are generally slightly weaker than those found in β-sheets. Thus, they are readily attacked by the surrounding molecules. In this study, both α-helix and β-sheets exhibit changes with added surfactant molecules. The interaction with C_8FONa leads to the greatest protein conformational changes (particularly at 70 and 90 °C), whereas C_8HONa leads to smallest changes. These findings suggest that the strength of the interactions between fibrinogen and the three surfactants followed the order C_8FONa > C_{12}HONa > C_8HONa. Previous studies have explained the different interactions between fibrinogen and ligands in terms of ligand molecular structure [36,37]. In this case, the most hydrophobic surfactants (C_8FONa, C_{12}HONa) were found to interact stronger with fibrinogen. On the other hand, because of the small size of C_8FONa, a greater number of molecules can interact with fibrinogen, and such interactions can be strong enough to cause the protein unfolding. Similar conclusion has been obtained by comparing the adsorption of β-endorphin and epinephrine to the different domains of the fibrinogen through electrostatic, polar, and hydrophobic interactions, resulting in protein unfolding, which may in turn expose the receptor-induced binding sites [38].

Difference absorption spectra of fibrinogen in the presence of different C_8HONa concentrations are presented in Fig. 4 (spectra corresponding to the other surfactants follow the same pattern). It is assumed that in the near-UV, the major factors responsible for the absorbance are tryptophan and tyrosine with a maximum at 280 nm [39]. Although fibrinogen contains appreciable amounts of phenylalanine, the perturbation spectrum of these residues is situated at a much shorter wavelength and has a much lower intensity than those of tyrosine and tryptophan and do not need to be considered here. The primary structure of fibrinogen contains a total of 72 tryptophan [40] and 88 tyrosine residues distributed along the molecule, with each Aα, Bβ, and γ chains having 21, 27, and 32 of these residues, respectively (NCBI Protein Database). Two isodichroic points, when the concentration of surfactant is varied, can be observed at 280 nm and 292 nm approximately. This fact reveals that two species are present in the solution [41]. Assuming that the surfactants do not contribute to the absorption spectrum, the two species should, indeed, correspond to different

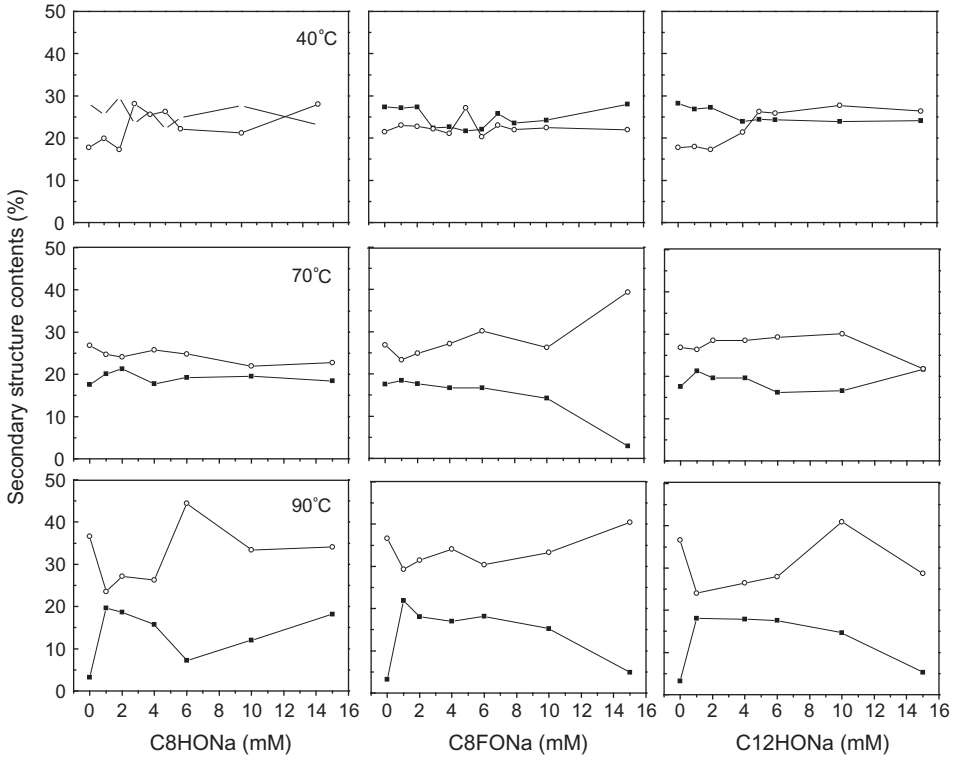

Fig. 3. Contents (in%) of the α-helix (■) and β-sheet (○) elements in fibrinogen as a function of surfactant concentration at different temperatures.

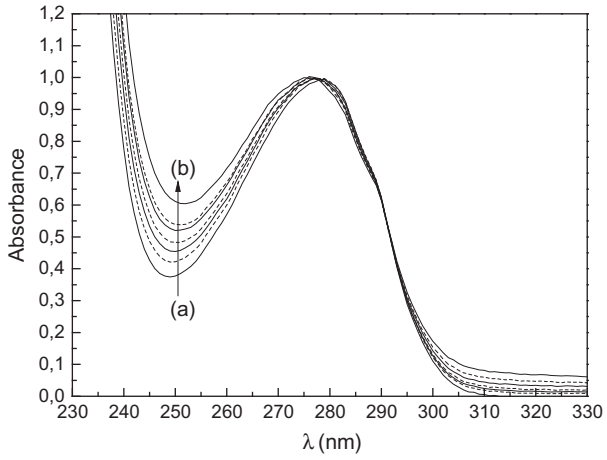

Fig. 4. Difference absorption spectra of fibrinogen (0.5 g dm^{-3}) in the presence of different C_8HONa concentrations from: 2 (a) to 16 mM (b).

unfolded states of the fibrinogen molecule, which is in good agreement with the cooperativity obtained from DSC measurements. There were no great changes in the overall shape of the adsorption spectra. Very slight decrease in the maximum region was noticed, but there was distinct increase in the minimum region. Shifts of 2–3 nm towards blue have been observed for C_8HONa and C_{12}HONa. Meanwhile, blue shift is only of 1 nm for C_8FONa. In a previous study, Guo et al. [42] have found a blue shift for different fibrinogen concentrations (without added surfactants), which has been attributed to concentration-dependent self-association where amino acid residues are exposed to an apolar environment. In our study, the protein concentration remains constant, so blue shift arises from the hydrophobic interactions of tryptophan with the hydrophobic moiety of the surfactants. Transition midpoints (T_m) were also checked by UV–vis showing a good agreement with those obtained from DSC.

In order to discuss how the surfactants affect the secondary structure of the protein, we have analyzed Raman spectra for fibrinogen in the presence of hydrogenated and fluorinated surfactants (Fig. 5). The band at 1641 cm^{-1} corresponds to the amide I band, which is sensitive to the secondary structure in fibrinogen. In the presence of surfactants, this band shifts slightly from 1641 cm^{-1} to 1648 cm^{-1}, 1651 cm^{-1}, and 1649 cm^{-1} for C_8FONa, C_8HONa, and C_{12}HONa respectively. These slight changes in the position (and intensity) of the amide I band indicate that the surfactant adsorption on protein is accompanied by changes in the secondary structure of the protein: from a high α-helix content to the β-sheet structure [43] (Fig. 5). These results correlated well with CD analysis.

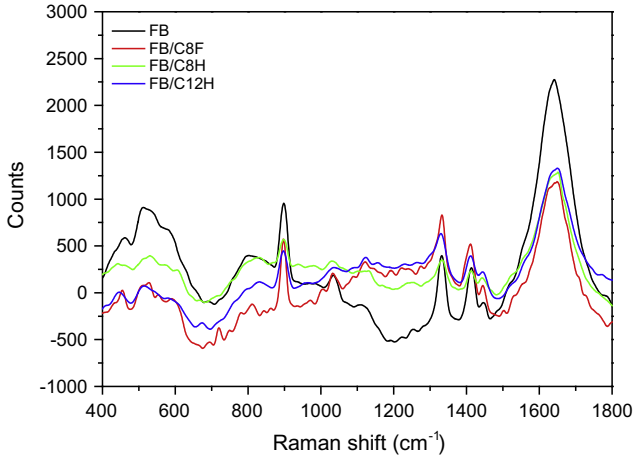

Fig. 5. Raman spectra of fibrinogen in presence of C_8FONa, C_8HONa, and C_{12}HONa.

At 1448 cm^{-1}, this band is assigned to the deformation modes of both CH_3 and CH_2 vibrations. The ratio of the Raman peak area of CH_3 and CH_2 deformation mode related to the Raman peak area of the amide I band (1641 cm^{-1}) is increasing from 0.0056 to 0.0170, 0.0115, and 0.0171 for C_8FONa, C_8HONa, and C_{12}HONa respectively. The decreasing Raman peak area of the amide I band is clearly observed in the presence of three surfactants. With these results, one can assume that the adsorption takes place via the amino acid side-chains, accompanied by changes in the secondary structure content but not in the overall structure of the protein.

3.2. SAXS analysis of fibrinogen in the absence and presence of surfactants

In the following, we describe the SAXS results with the aim of better understanding how the surfactant interaction impacts on the fibrinogen quaternary conformation at room temperature (T = 22 °C), *i.e.*, on the native fibrinogen structure. First of all, in the absence of surfactants, Fig. 6 shows the scattering intensity, normalized by the protein concentration, of fibrinogen at 1, 3, and 6.6 g dm^{-3} in the presence of 50 mM glycine–NaOH buffer, pH 8.5. SAXS measurements from samples composed of 0.5 g dm^{-3} did not result in any detectable SAXS signal (data not shown). However, the normalized scattering curves are practically the same for the three studied concentrations. Such a fact evidences that the protein conformational state is concentration-independent from 1 to 6.6 g dm^{-3}. Moreover, effects of interaction between proteins do not take place over the SAXS curves ($S_M(q)$ = 1 in the Eq. (2)) once they do not present any interference peak [22]. Therefore, we calculate $P(q)$ through the fibrinogen crystallographic structure as a disulfide-linked dimer of three nonidentical polypeptide chains (Fibrinogen Scheme 1), but the corresponding scattering curve fails to fit the experimental data at low q values (dashed line in the inset on Fig. 6). On the other hand, the scattering of a paired-dimer configuration as found in the crystallographic native structure (pdb code: 3GHG, depicted in the inset on Fig. 6) reproduces quite well the data (solid line in the inset on Fig. 6). So, the SAXS curves are compatible to the scattering of paired-dimers (arrangement of two FB dimers) in this studied concentration range.

Therefore, we decide to proceed with the investigation by using a protein concentration of 3 g dm^{-3}. In terms of surfactant concentration, we studied the influence of 60 mM of each surfactant on the fibrinogen structure. Note that such a concentration keeps the same molar ratio used in the DSC and spectroscopic measurements as 0.5 g dm^{-3} and 10 mM of surfactant.

Interestingly, the samples composed of hydrogenated surfactants C_8HONa and C_{12}HONa, in the absence of protein, did not produce any detectable scattering signal at 60 mM. Such a fact is easily understood because C_8HONa micelle-like aggregates are not expected to be formed at this concentration (CMC of 380 mM). In respect to C_{12}HONa (CMC of 27 mM), a quite small number of micelles must be self-assembling in solution but they are not detectable by our experimental setup. On the other hand, the fluorinated surfactant, C_8FONa, shows clearly a typical scattering curve from surface charged micelle-like aggregates [23] (Fig. 7), although it has a CMC value similar to that of C_{12}HONa. The presence of CF_2 group in the hydrophobic medium contributes to a larger extent to the electron density contrast in $P(q)$ form factor (Eq. (2)) than does the CH_2 group, even though the number of scattering particles n_p is small.

The analysis of the scattering curve from C_8FONa micelles, by assuming that the micelle shape can be described as a prolate ellipsoid-like aggregate (solid line in Fig. 6), resulted in a value of R_{par} = 11.5 Å that is compatible to the CH_3–$(CH_2)_7$ extended-chain length. Moreover, the anisometry ν (ratio between the longest and the smallest axes), the polar shell thickness, σ, and its electron density ρ_{pol} were equal to 2, 3.5 Å, and 0.40 e/Å^3, respectively. The hydrophobic volume of the surfactant was determined as 340 Å^3, in accordance with the value reported in the literature [44] of 343 Å^3. An aggregation number of 35 was then calculated in good agreement with the value found in the literature of 50 ± 21 [45]. From $S_M(q)$ modeling, 14e charges were found in the micellar surface, indicating that ca. 40% of the surfactants in the aggregate are ionized, in very good agreement with 39% determined for cesium perfluorooctanoate [42].

Concerning the influence of the surfactants on the fibrinogen structure, Fig. 8 shows the SAXS curves of 3 g dm^{-3} of protein in the absence and presence of 60 mM of C_8HONa, C_8FONa, and C_{12}HONa. The scattering curves are displayed in log scale in the inset on Fig. 8 to emphasize the differences. As one can observe, the presence of C_8HONa did not promote any significant change in fibrinogen scattering curve. Therefore, our results give support to conclude that the presence of C_8HONa molecules below CMC do not affect significantly the protein conformation that remains in its paired-dimer state, although small (or even subtle) local changes in the domains may be occurring according to DSC and spectroscopic measurements.

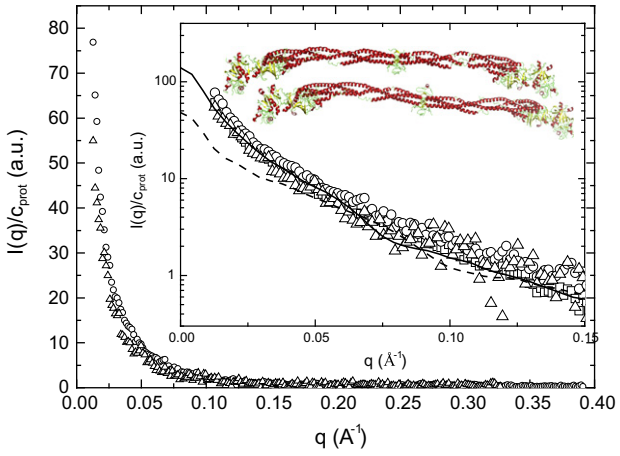

Fig. 6. SAXS curves normalized by the protein concentration, c, at three different values: 1 (open triangle), 3 (open circle), and 6.6 (open square) g dm^{-3}. Inset: theoretical scattering curves corresponding to the protein crystallographic structure (code 3GHG from PDB website) from the paired-dimer (solid line) and the dimer (dashed line) configuration. See text for details.

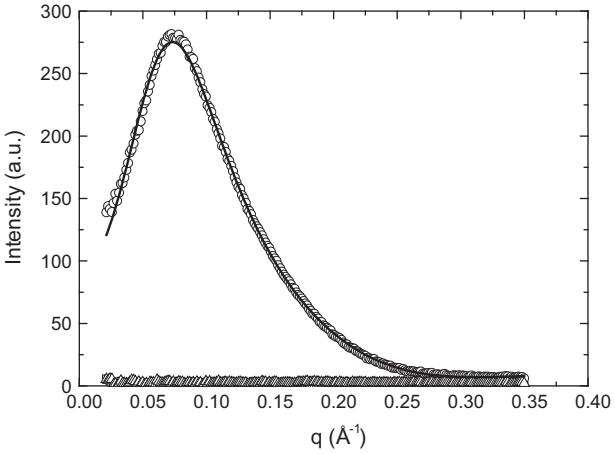

Fig. 7. SAXS curves of 60 mM of C_8FONa (open circles) and C_{12}HONa (open triangles) for comparison, at 50 mM glycine-NaOH buffer solution, pH 8.5. The solid line represents the best fit obtained with the prolate ellipsoidal model to C_8FONa SAXS data. The fitting parameters are described in the text.

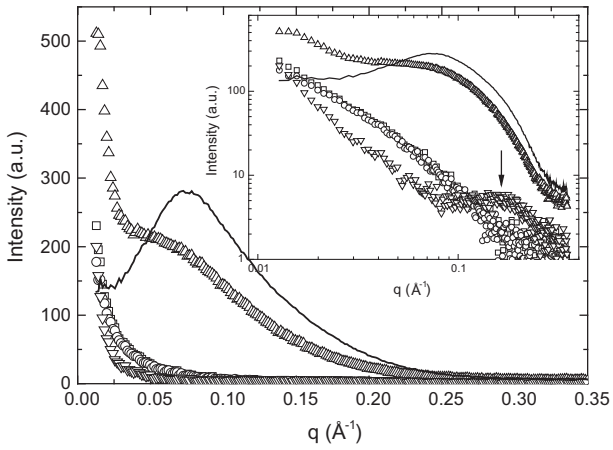

Fig. 8. SAXS curves of bovine fibrinogen (3 g dm^{-3}) in the absence (open squares) and presence of 60 mM of C_8HONa (open circles), C_8FONa (open triangles), and C_{12}HONa (open inverted triangle). Inset: the scattering curves are shown in log scale to remark the differences. The solid line represents the scattering curve of 60 mM C_8FONa in protein-free solution (Fig. 7) for comparison purpose.

On the other hand, the presence of fluorinated surfactants (C_8FONa) alters the scattering profile. There is an increase in the intensity in the small q region concomitantly with the appearance of a shoulder around 0.08 Å^{-1} (Fig. 8) related to the fluorinated surfactant micelle formation. The scattering profile is indeed due to a sum (solid line on Fig. 9) of two independent scatterings: one is due to the FB in the paired-dimer configuration and the other one to the fluorinated surfactant micelles coexisting in solution. The structural parameters from the FB and the micelles previously analyzed, Figs. 6 and 7, remain practically the same. Just the micelle ionization coefficient is reduced from 40% to 30%. Knowing that the fibrinogen pI (isoelectric point) is 5.5, at pH 8.5, the protein has a negative net charge in such a way that there are a large number of cationic counterions in the bulk in order to keep the electro-neutrality. As a consequence, some positive counterions must be screening the micelle surface charge. Therefore, our SAXS results indicate that at 60 mM, C_8FONa monomers may interact with fibrinogen paired-dimer without promoting dissociation or significant conformational changes, whereas micelle-like aggregates coexist in solution. Small local changes in the secondary structure of the fibrinogen as evidenced by DSC and spectroscopic measurements are not reflected in the overall protein conformation as seen by SAXS at room temperature.

Finally, the presence of sodium dodecanoate changes the scattering profile of the protein and induces the appearance of a broad peak around $q \approx 0.17$–0.18 Å^{-1} (black arrow in the inset on Fig. 8), which is related to the formation of micelle-like aggregates in solution similar to those formed by sodium dodecyl sulfate [15]. Therefore, our results evidence that the presence of fibrinogen favors the formation of C_{12}HONa micelle-like aggregates at concentrations lower than CMC of the surfactant in protein-free solution, as previously reported for other proteins and sodium alkyl sulfates [15,16]. Further, the fibrinogen scattering is also modified. Nevertheless, in this case, the SAXS curve is not well represented by the sum of the two independent scatterings related to the protein and the micelles. In fact, the micelles probably grow around specific hydrophobic regions of fibrinogen, inducing changes in the protein conformation as we explore below.

Different models have been described with the aim of monitoring the complexation between proteins and surfactants as "*pearl necklace model*" [15,16,46,47] and "*polypeptide unfolded chain wrapping around micelles*" [48]. However, the three polypeptide chains of fibrinogen are held together by 29 disulfide bonds [49]. These chains conserve secondary structure in the presence of the three surfactants as it has been demonstrated by CD measurements. Thus, fibrinogen complexes cannot behave as flexibly as a random coil. For this reason, we analyzed the SAXS curve of bovine fibrinogen (3 g dm^{-3}) in the presence of C_{12}HONa through the $p(r)$ function [16]. Fig. 10 shows the SAXS data along with the best fit obtained with the GIFT software [26] corresponding to the $p(r)$ function shown in the inset on Fig. 10. The first oscillation in the $p(r)$ function for $r < 50$ Å is a fingerprint of micelle formation [16], while the following maxima are associated with micelle dimension and the mean distance between two adjacent micelles. Accordingly, these values are equal to 57 Å and 138 Å, respectively. The micelle dimension is compatible to the values reported for sodium alkyl sulfate micelles [15,16]. Furthermore, the extension of the protein–surfactant complex can be inferred from the position where $p(r)$ goes to zero and amounts to ca. 400 Å. Such a value is near the FB longest dimension (see Fibrinogen Scheme 1). Based on this model, we may infer that C_{12}HONa interacts with the protein, forming a complex, where probably micelle-like aggregates are locally assembled at some hydrophobic moieties of the polypeptide chains.

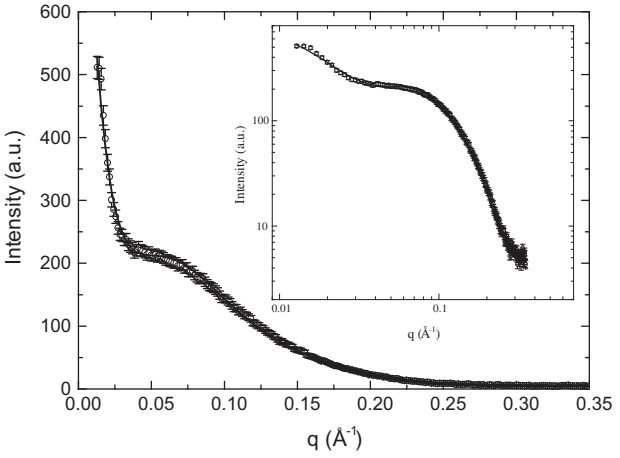

Fig. 9. SAXS data of fibrinogen 3 g dm^{-3} in the presence of 60 mM of C_8FONa (open circles): the data are well fitted as a sum of independent scatterings due to paired-dimers FB and fluorinated surfactant micelles. The same scattering data can be appreciated in the log scale in the inset.

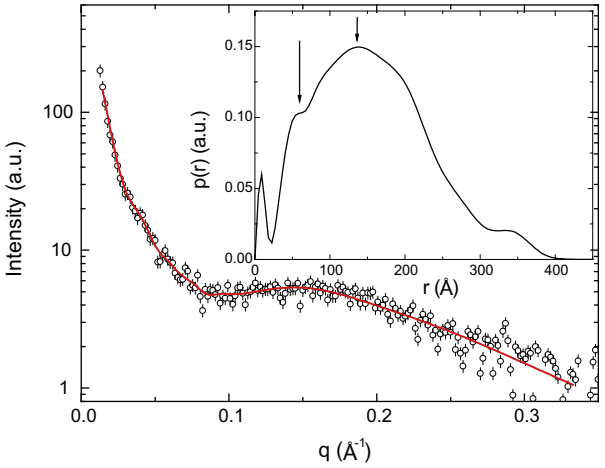

Fig. 10. SAXS curve of fibrinogen 3 g dm^{-3} in the presence of 60 mM of C_{12}HONa in the glycine buffer. The solid line represents the best fit obtained with the GIFT software [26], and the correspondent $p(r)$ function can be appreciated in the inset. The arrows indicate the micelle diameter (equal to 57 Å) and the micelle–micelle mean distance (equal to 138 Å). See text for details.

4. Conclusions

The supramolecular assembly between bovine fibrinogen and sodium perfluorooctanoate, octanoate, and dodecanoate in buffer solution has been studied using different experimental techniques and theoretical models. The results obtained are summarized as follows. As a first step, we have studied the thermal stability of fibrinogen in the presence of the surfactants. Addition of hydrogenated surfactants results in decrease in melting temperatures. However, the fluorinated plays two opposite roles in the folding and stability of fibrinogen: acting as a structure stabilizer at low molar concentrations (enhancing T_m) and as a destabilizer at higher concentrations (diminishing T_m). Unfolding process of fibrinogen does not follow a two-state process but involves intermediate states for all studied systems. Increasing temperature and/or surfactant concentration results in a decrease in α-helix (and β-sheet increase) content. However, both the quaternary and tertiary structure does not undergo large variations as can be inferred from UV–vis and Raman spectra. SAXS measurements have shown that pure fibrinogen exists as a paired-dimer in this medium. In the presence of surfactant, the map of the configurations of the protein changes, depending on the hydrophobicity of surfactant. The presence of C_8HONa (lowest hydrophobicity) did not promote any significant change in fibrinogen. C_8FONa monomers interact with fibrinogen paired-dimer without promoting dissociation or significant conformational changes. On the other hand, the interaction between C_{12}HONa (highest hydrophobicity) and the protein promotes the surfactant self-assembling at hydrophobic moieties. Finally, we would like to point out that the picture of the fluorocarbon/hydrocarbon plus fibrinogen system reported here could provide a key that paves the way for future biochemical and biomedical applications, for example, in the recovery of proteins and protein conformation on support materials for regenerative therapies.

Acknowledgments

The authors thank the Xunta de Galicia for financial support (Project No. PXI20615PN). Authors also thank Prof. J.L. Mascareñas (Department of Organic Chemistry, University of Santiago de Compostela) for the use of CD spectrometer equipment. RI and LRSB thank Fundação de Amparo à Pesquisa do Estado de São Paulo (FAPESP) for financial support. RI also acknowledges Conselho Nacional de Pesquisa (CNPq) for research fellowship.

References

[1] O. Svensson, K. Thuresson, T. Arnebrant, Langmuir 24 (2008) 2573.
[2] J.J. Feng, P. Hildebrandt, D.H. Murgida, Langmuir 24 (2008) 1583.
[3] M.J. Meziani, Y.P. Sun, J. Am. Chem. Soc. 125 (2003) 8015.
[4] D.N. Petsev, P.G. Vekilov, Phys. Rev. Lett. 84 (2000) 1339.
[5] D. Zhong, A. Douhal, A.H. Zewail, Proc. Natl. Acad. Sci. 97 (2000) 14056.
[6] J.H. Brown, N. Volkmann, G. Jun, A.H. Henschen-Edman, C. Cohen, Proc. Natl. Acad. Sci. 97 (2000) 85.
[7] S. Yakovlev, L. Medved, Biochemistry 48 (2009) 5171.
[8] G. Tsurupa, R.R. Hantgan, R.A. Burton, I. Pechik, N. Tjandra, L. Medved, Biochemistry 48 (2009) 12191.
[9] A. Rieux, A. Shea, L.D. Shea, J. Controlled Release 136 (2009) 148.
[10] R. Uibo, I. Laidmäe, E.S. Sawyer, L.A. Flanagan, P.C. Georges, J.P. Winer, P.A. Janmey, Biochim. Biophys. Acta 1793 (2009) 924.
[11] I. Keere, R. Willaert, A. Hubin, J. Vereecken, Langmuir 24 (2008) 1844.
[12] L.C. Xu, C.A. Siedlecki, Langmuir 25 (2009) 3675.
[13] (a) E.L. Gelamo, M. Tabak, Spectrochim. Acta Part A 56 (2000) 2255;
(b) W. Cong, Q. Liu, Q. Liang, Y. Wang, G. Luo, Biophys. Chem. 143 (2009) 154.
[14] J.H. Hansen, S.V. Petersen, K.K. Andersen, J.J.E.T. Damhus, D. Otzen, Biopolymers 91 (2008) 221.
[15] (a) S.F. Santos, D. Zanette, H. Fischer, R. Itri, J. Colloid Interface Sci. 261 (2003) 400;
(b) B. Shweitzer, D. Zanette, R. Itri, J. Colloid Interface Sci. 277 (2004) 285.
[16] M. Ospinal-Jiménez, D.C. Pozzo, Langmuir 27 (2011) 928.
[17] (a) J.M. Ruso, P. Taboada, P. Martinez-Landeira, G. Pieto, F. Sarmiento, J. Phys. Chem. B 105 (2001) 2644;
(b) J.M. Ruso, N. Deo, P. Somasundaran, Langmuir 20 (2004) 8988.
[18] E. Chabaud, P. Barthelemy, N. Mora, J.L. Popot, B. Pucci, Biochimie 80 (1998) 515.
[19] P. Raychaudhuri, Q. Li, A. Mason, E. Mikhailova, A.J. Heron, H. Bayley, Biochemistry 50 (2011) 1599.
[20] E. Blanco, A. González-Pérez, J.M. Ruso, R. Pedrido, G. Prieto, F. Sarmiento, J. Colloid Interface Sci. 288 (2005) 247.
[21] (a) A. Lobley, L. Whitmore, B.A. Wallace, Bioinformatics 18 (2002) 211;
(b) L. Whitmore, B.A. Wallace, Nucleic Acids Res. 32 (2004) W668.
[22] L.R.S. Barbosa, M.G. Ortore, F. Spinozzi, P. Mariani, S. Bernstorff, R. Itri, Biophys. J. 98 (2010) 147.
[23] (a) L.R.S. Barbosa, W. Caetano, R. Itri, P. Homem-de-Mello, P.S. Santiago, M. Tabak, J. Phys. Chem B 110 (2006) 13086;
(b) W. Caetano, L.R. S Barbosa, R. Itri, M. Tabak, J. Colloid Interface Sci. 260 (2003) 414.
[24] (a) J.B. Hayter, J.B. Penfold, Mol. Phys. 42 (1981) 109;
(b) J. Hayter, J. Penfold, J. Chem. Soc. Faraday Trans. 1 77 (1981) 1851;
(c) J.P. Hansen, J.B. Hayter, Mol. Phys. 46 (1982) 651.
[25] P.T. Campana, L.R.S. Barbosa, R. Itri, Int. J. Biol. Macromol. 48 (2011) 398.
[26] A. Bergmann, G. Fritz, O. Glatter, J. Appl. Crystallogr. 33 (2000) 1212.
[27] Y. Chen, H. Mao, X. Zhang, Y. Gong, N. Zhao, Int. J. Biol. Macromol. 26 (1999) 129.
[28] P.L. Privalov, L.V. Medev, J. Mol. Biol. 159 (1982) 665.
[29] J.W. Donovan, E. Mihalyi, Proc. Natl. Acad. Sci. USA 71 (1974) 4125.
[30] Y. Moriyama, K. Takeda, Langmuir 15 (1999) 2003.
[31] A.W.P. Vermeer, W. Norde, Colloid Surf., A 161 (2000) 139.
[32] (a) A. Cooper, M.A. Nutley, A. Wadood, Differential Scanning Microcalorimetry in Protein–Ligand Interactions: Hydrodynamics and Calorimetry, in: S.E. Harding, B.Z. Chowdhry (Eds.), Oxford University Press, Oxford, 2001;
(b) S. Deep, J.C. Ahluwalia, Phys. Chem. Chem. Phys. 3 (2001) 4583.
[33] L. Razumovsky, S. Damodaran, Langmuir 15 (1999) 1392.
[34] N. Ohta, T. Totsuyanagi, Biol. Pharm. Bull. 16 (1993) 631.
[35] I. Azpiazu, D. Chapman, Biochim. Biophys. Acta 1119 (1992) 268.
[36] S. Martini, M. Consumi, C. Bonechi, C. Rossi, A. Magnani, Biomacromolecules 8 (2007) 2689.
[37] C. Bonechi, S. Martini, C. Rossi, Bioorg. Med. Chem. 17 (2009) 1630.
[38] R. Barbucci, S. Lamponi, A. Magnani, Biomacromolecules 4 (2003) 1506.
[39] J.R. Lakowicz, Principles of Fluorescence Spectroscopy, Kluwer Academic/Plenum Publishers, New York, 1999.
[40] S. Goncalves, N.C. Santos, J. Martins-Silva, C.J. Saldanha, Photochem. Photobiol. B: Biol. 86 (2007) 170.
[41] K.A. Connors, Binding Constants: The Measurements of Molecular Complex Stability, Wiley, New York, 1987.
[42] J. Guo, N. Harn, A. Robbins, R. Dougherty, C.R. Middaugh, Biochemistry 45 (2006) 86.
[43] G.J. Thomas, Biophys. J. 46 (1984) 763.
[44] S.S. Berr, R.R.M. Jones, J. Phys Chem. 93 (1986) 2555.
[45] H. Iijima, T. Kato, H. Yoshida, M. Imai, J. Phys. Chem. B 102 (1998) 990.
[46] K. Shirahama, K. Tsujii, T. Takagi, J. Biochem. 75 (1974) 309.
[47] S.H. Chen, J. Teixeira, Phys. Rev. Letter 57 (1986) 2583.
[48] A. Chakraborty, D. Seth, P. Setua, N. Sarkar, J. Phys. Chem. B 110 (2006) 16607.
[49] A. Henschen, J. McDonagh, Fibrinogen, fibrin and factor XIII, in: R.F.A. Zwaal, H.C. Hemker (Eds.), Blood Coagulation, Elsevier Science, Amsterdam, 1986.